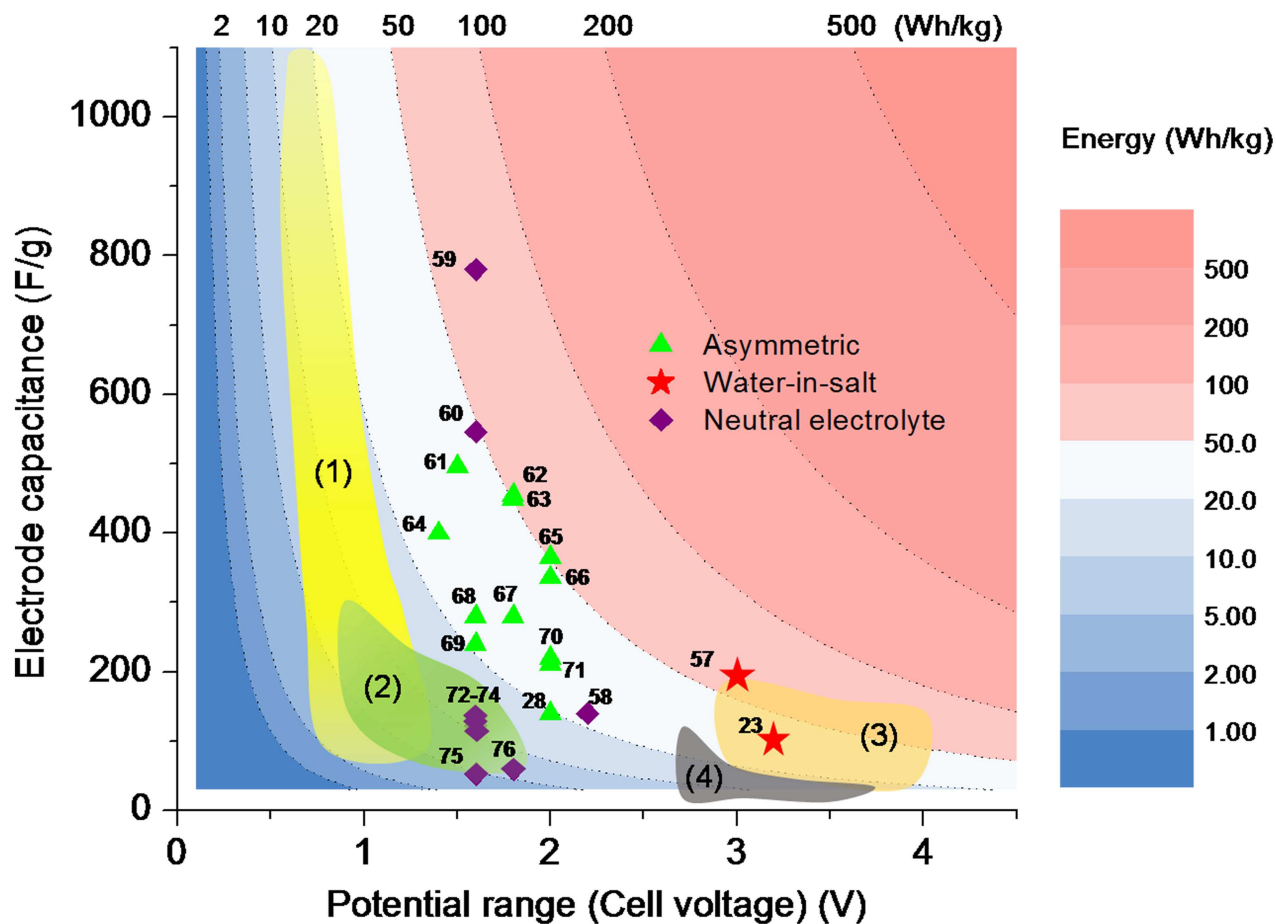




High-Voltage Supercapacitors Based on Aqueous Electrolytes

Xining Zang^{+, [a, b]} Caiwei Shen^{+, *[a, c]} Mohan Sanghadasa,^[d] and Liwei Lin^{*[a]}



Supercapacitors with high power density and life cycles are an important family of power supplies among energy storage systems. The operating voltage window of a supercapacitor is determined by both the chemistry of electrode materials and the electrochemical kinetics of electrolytes while the water hydrolysis potential of 1.23 V is the typical limit for capacitors based on aqueous electrolytes. Here, we briefly outline the working mechanism of electrochemical supercapacitors, including electron double layer capacitors (EDLC) and pseudo-

capacitors, and investigate the limitations of their working voltages. The principles and examples of different designs of electrodes and electrolytes for high-voltage supercapacitors beyond the hydrolysis limit are discussed, such as asymmetric electrodes, high concentration electrolytes, and electrolytes with different pH values. Insights into high voltage capacitor cells and future prospects are provided for the development of electrochemical energy storage systems.

1. Introduction

Energy storage devices have become increasingly important because of the demands in rapidly advancing technologies such as portable/wearable electronics, electrical vehicles, drones, internet of things, point-of-care medical systems, renewable energy systems, and so on.^[1,2] While lithium-ion batteries (LIBs) are the power solution for most of the current consumer electronics and electric vehicles because of its relatively high energy density and power density, further developments are desirable to enhance the safety, durability and lower the manufacturing cost of the current and future power systems.^[3–6]

Supercapacitors, also called electrochemical capacitors or ultracapacitors, are energy storage devices providing higher power density, longer cycle life, and safer operation when compared with LIBs.^[7,8] The combinations of supercapacitors with LIBs have already been widely applied to improve the overall power performances of the existing electrical devices and systems.^[4,6] On the other hand, supercapacitors have attracted research interests in various fields, including micro self-powering systems^[9–11] and renewable energy systems,^[12] as the long cycle-ability and high-power handling ability are critical in energy harvesters/generators.^[13] Specifically, in flexible and wearable electronics, the mechanical durability and safety of the power sources are of high interests^[14,15] and supercapacitors could provide new and unique solutions.^[16,17]

Unlike battery systems, the maximum energy that can be stored in a capacitive device is proportional to the capacitance multiplies the square of the operation voltage. Current commercial supercapacitors have been using nonaqueous electrolytes to

achieve high operation voltages for high energy storage capacities. However, aqueous electrolytes can offer good advantages such as: (1) higher ionic conductivity ($> 100 \text{ mS/cm}$) than those of nonaqueous ones ($\sim 1 \text{ mS/cm}$) for high power density; (2) non-flammable and safe operations; (3) low material cost; and (4) potential low manufacturing cost without the fabrication requirement in water-free environment.^[7,18]

However, aqueous electrolytes suffer from one major drawback: low operation voltage, which limits the energy density. The thermodynamic decomposition voltage of water is 1.23 V and researchers have been using this number as the operation limit. In practice, a voltage higher than 1.23 V may not decompose water because of two fundamental reasons. First, an overpotential is required for the hydrogen/oxygen evolution processes on any electrode surface^[19–21] and the overpotential magnitude can vary a lot for different electrode materials. Second, the interaction between ions and solvents in electrolytes increases the difficulty for the water decomposition process.^[22,23] By utilizing these two mechanisms, a variety of electrode-electrolyte systems for supercapacitors have been designed and demonstrated for high voltages operations.

While aqueous supercapacitors with high working voltage are attractive, the understanding of the fundamental mechanisms has been lacking and the standard procedures to determine the proper operation voltage for a certain system haven't been well established. In this paper, we summarize the previously reported aqueous supercapacitors working at high voltages ($> 1.23 \text{ V}$), including mechanisms, characterization approaches, materials and configurations with future outlooks.

2. Theoretical Background

2.1. Working Mechanisms of Supercapacitors

Conventional capacitors store charges on two metal plates separated by a dielectric layer with two typical types, the parallel-plate capacitor (Figure 1a) and electrolytic capacitor (Figure 1b). Both systems provide capacitances that are proportional to the area of the electrodes, and inversely proportional to the thickness of the dielectric layer.^[9] Electrochemical supercapacitors, however, store charges based on the electrochemical double layer (EDL) effect and/or pseudo capacitance effect.^[7,8] In an EDL capacitor (Figure 1c), static charges are separated at the electrode-electrolyte interface by a distance of less than 1 nm. The pseudo capacitor (Figure 1d) also stores

[a] Dr. X. Zang,⁺ Prof. C. Shen,⁺ Prof. L. Lin

Mechanical Engineering
University of California Berkeley
Berkeley, CA, USA, 94704
E-mail: lwl@berkeley.edu
cshen2@umassd.edu

[b] Dr. X. Zang⁺
Research Laboratory of Electronics, Massachusetts Institute of Technology,
Cambridge, MA, USA, 02139
E-mail: xzang@mit.edu

[c] Prof. C. Shen⁺
Mechanical Engineering Department
University of Massachusetts, Dartmouth,
MA, USA, 02747

[d] Dr. M. Sanghadasa
Aviation and Missile Research,
Development, and Engineering Center,
US Army, Redstone Arsenal, AL, USA, 35898

[+] Authors contribute equally to this paper

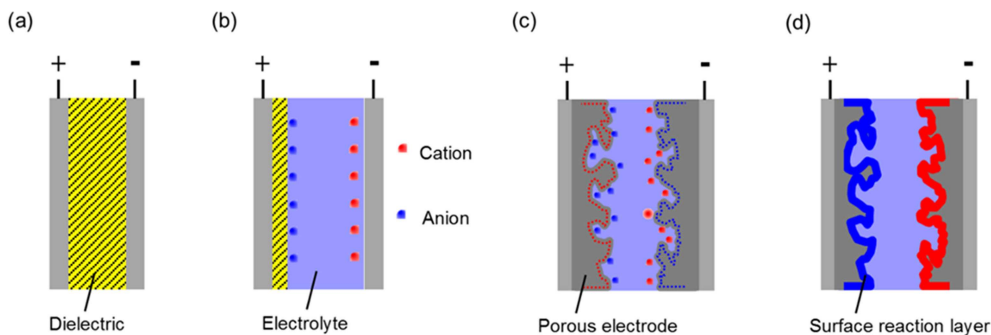


Figure 1. Schematics of the working principles of four types of capacitors: (a) parallel-plate capacitor, (b) electrolytic capacitor, (c) EDL capacitor, and (d) pseudo capacitor. EDL capacitor and pseudo capacitor are also called supercapacitors because they have much larger capacitance than those of the other capacitors.^[9] Copyright 2017, IEEE.

charges at the electrode-electrolyte interface but it also has the reversible redox reactions for an added derivative capacitance. Such mechanisms result in volumetric/gravimetric capacitances that are much larger (can be 10,000 times larger) than those of conventional capacitors.

The maximum operating voltages of the capacitive charge storage devices are limited by the breakdown phenomena. In conventional capacitors, the high electric field may cause the breakdown of the dielectric layer and short the two electrodes.

In supercapacitors, ions/electrons may go across the electrode-electrolyte interface and react irreversibly. The latter phenomenon happens at voltages lower than those of conventional capacitors, as the positive and negative charges are much closer to each other in supercapacitors.



Dr. Xining Zang is a postdoc associate in Research Laboratory of Electronics (RLE) in Massachusetts Institute of Technology. Dr. Zang got her PhD from University of California Berkeley in 2017 August. During PhD she worked in Prof Liwei Lin group, on 2D materials synthesis and assembly to nanostructured device. Her current research focus on wafer scale manufacturing and integration of 2D materials including transition metal chalcogenide and transition metal carbides for electronics and energy related applications (catalyst, battery and supercapacitors).



Prof. Caiwei Shen, Prof. Caiwei Shen received the Ph.D. degree in mechanical engineering from University of California at Berkeley in 2018. He is currently an assistant professor with mechanical engineering department in the University of Massachusetts Dartmouth. His research interests include nanomaterials for energy and electronics related applications, integrated energy storage, and multifunctional composites.



Dr. Mohan Sanghadasa was with the Faculty of University of Alabama, Huntsville (UAH), for 12 years. He is currently a Senior Research Scientist with the AMRDEC, U.S. Army. He also leads research programs on the development of nanotechnology enhanced sensors and energy storage systems. During his academic career, he has also conducted research on optical limiting, optical switching, and optical pattern recognition. His research activities with UAH were primarily in the area of non-

linear optics. His research activities with AMRDEC were on the development of micro devices, and polymer based modulators for IFOGs in inertial measurement units.



Prof. Liwei Lin received the Ph.D. degree in mechanical engineering from the University of California at Berkeley (UC-Berkeley) in 1993. He joined UC-Berkeley in 1999, where he is currently a Professor with the Mechanical Engineering Department and a Co-Director with the Berkeley Sensor and Actuator Center. He has 20 issued U.S. patents in the area of MEMS/NEMS. His research interests are in design, modeling and fabrication of micro/nano structures, micro/nano sensors and micro/nano actuators, mechanical issues in micro/nano systems including heat transfer, and solid/fluid mechanics and dynamics. He is an ASME Fellow. He was a recipient of the 1998 NSF CAREER Award for research in MEMS packaging and the 1999 ASME Journal of Heat Transfer Best Paper Award for his work on micro scale bubble formation. He led the effort to establish the MEMS Division in ASME and served as the Founding Chairman of the Executive Committee from 2004 to 2005. He was the general Co-Chair of the IEEE 24th international conference on Micro Electro Mechanical Systems in 2011. He currently serves as a Subject Editor of the IEEE/ASME Journal of Microelectromechanical Systems and the North and South America Editor of the Sensors and Actuators-A Physical.

2.2. Limitations of Operation Voltage of Aqueous Supercapacitors

As supercapacitors can store charges reversibly, they fail to work properly when irreversible electrochemical processes happen. Therefore, the operation voltage of a supercapacitor cell is limited by the reversible electrochemical window of its two electrodes, which is defined as the *potential range* in this paper. The *voltage of a supercapacitor cell* is calculated as the potential difference between positive and negative electrodes. The supercapacitor cell is supposed to be *operational* only when both electrodes are within the proper potential range.

Assuming that the lower potential limit of the negative electrode is E_{N1} and the upper potential limit of the positive electrode is E_{P2} , the maximum cell voltage should be no more than $E_{P2}-E_{N1}$.^[24] The typical electrochemical processes and their limits on E_{N1} and E_{P2} are reviewed in this section.

2.2.1. Water Decomposition

The water decomposition process is irreversible in an aqueous supercapacitor. The reaction can be chemically expressed as the following:



In an electrochemical cell, such a process is divided into two parts on the positive and negative electrode, respectively. At the positive electrode, oxygen evolution reaction (OER) happens:



At the negative electrode, hydrogen evolution reaction (HER) happens:



The minimum potential difference (ΔE^0), or cell voltage, to make the water decomposition happen can be calculated by a thermodynamic approach:

$$\Delta G = -nF\Delta E^0, \quad (4)$$

where ΔG is the Gibbs free energy change in the process; n is the number of electron transferred; and F is the Faraday constant. The ΔE^0 is calculated to be 1.23 V at 25 °C and 1 atm for the water decomposition process.^[21,25] However, the actual electrochemical process is more complicated on the electrode-electrolyte interface. For example, the HER can involve three possible steps in acidic media.^[25] The first one is the Volmer step: $\text{H}^+ + \text{e}^- \rightarrow \text{H}_{\text{ads}}$, in which an adsorbed hydrogen atom (H_{ads}) on the electrode surface is produced. Then the HER can proceed by the Tafel step ($2\text{H}_{\text{ads}} \rightarrow \text{H}_2$), or the Heyrovsky step ($\text{H}_{\text{ads}} + \text{H}^+ + \text{e}^- \rightarrow \text{H}_2$), or both. If the H_{ads} is attached strongly on the electrode, some excess potential (known as overpotential, η) has to be applied to overcome the additional free energy

change due to hydrogen adsorption (ΔG_{H}), so that HER can proceed. It is also true that an overpotential has to be applied for OER to happen. The value of overpotential varies for different electrode surfaces and solutions with different pH values. Another phenomenon that further increases the overpotential for water decomposition is the interaction of solvated ions with water molecules. Such interaction can be more significant in water solutions with higher ion concentration.^[22,23] In addition, the ionic and electrical resistances of the solution and electrode may also increase the required overpotential.^[26]

As a result, the actual potential difference that can decompose water should be:

$$\Delta E = \Delta E^0 + \eta_p + \eta_n + \eta_{\text{other}} \quad (5)$$

where η_p and η_n are overpotentials applied on the positive and negative electrode, respectively, and η_{other} represents the overpotential from the solution, the resistances, and so on. The combination of selected positive and negative electrodes and electrolyte can greatly increase the voltage needed for water decomposition.

2.2.2. Limitations for EDLC Electrodes

EDLCs mainly use nanostructured carbon materials as electrodes because they can provide very high surface areas and possess the highest specific capacitances (100–200 F/g). Carbon can't be easily reduced unless there are oxygen-containing functional groups on the surface. Still, the lowest working potential for carbon electrodes in aqueous electrolyte is usually limited by the potential of HER. Different types of carbon nanomaterials show different overpotentials for HER, but the values are generally high. Therefore, carbon nanomaterials are widely used as the negative electrode materials in various asymmetric supercapacitor systems to expand the potential limit.^[26–28] The oxidation of carbon can occur for nanoporous carbon materials with lots of defects, such as activated carbon and reduced graphene oxide and surface functional groups on carbon can be produced in the oxidation process.^[27,28] Such reactions can happen before OER, and limit the highest working potential for carbon-based electrodes. The exact potential limit varies by the types of carbon as well as the process to produce and assemble the materials. While the surface functional groups cannot be completely removed from most of the carbon materials, they sometimes play a positive role to introduce additional reversible pseudocapacitance for the EDL electrodes.^[29,30]

2.2.3. Limitations for Pseudocapacitive Electrodes

The pseudocapacitive electrodes can provide higher capacitance than those of EDLC electrodes, but they usually work within a narrower potential range, smaller than that of the water decomposition limit. The reason is that redox reactions leading to a pseudocapacitive effect are only reversible within a certain potential range. Further reduction/oxidation of the electrodes can

cause irreversible effects that don't provide the capacitive behavior. As one category of pseudocapacitive materials, transition metal oxides such as RuO₂ and MnO₂ have been intensively studied. RuO₂ has three distinct oxidation states accessible within 1.2 V in acidic electrolytes, and the Ru oxidation states can change from (ii) up to (iv) continuously.^[5,6] RuO₂ shows different reactions in electrolytes with different pH value,^[31] but its potential range is still limited by the reversible oxidation states. MnO₂ has theoretically comparable capacitance (~1300 F/g) as RuO₂, but its capacitive potential range is slightly smaller (<1 V).^[30] Moreover, MnO₂ is very unstable as negative electrode because it can be reduced to Mn²⁺ and dissolved in the electrolyte.

In recent years, metal sulfides, carbides, and nitrides with 2D layered structures have been proposed as pseudocapacitive electrode materials with considerably high (especially volumetric) capacitances (up to 900 F/cm³).^[32] Although such 2D materials offer large surface-area-to-volume ratios and less solid-state diffusion effects, their potential ranges are limited by the reversible reaction potentials, which are only 0.5~0.9 V in representative reports.^[32–34]

Conducting polymers are another type of widely used pseudocapacitive materials which store charges based on a reversible doping/un-doping process of ions into the polymer matrix.^[35–37] The potential window of conducting polymer is generally determined by the polymer degradation process at a positive potential and the switching to an insulating state (undoped state) at a negative potential during the discharge process of the electrode. Some pseudocapacitive conducting polymers including polypyrrole and polyaniline show measured capacitances up to 500 F/g, but their reversible potential ranges are only 0.7~0.8 V.^[36]

2.3. Experimental Determination of Potential Range and Working Voltage

The exact reversible potential ranges of electrodes are difficult to predict by theoretical calculations, as the electrochemical processes in a real supercapacitor cell can be complicated. Therefore, the potential range of an electrode and the operation voltage of a supercapacitor cell are always experimentally determined but the measurement procedure is not standardized. A few techniques are discussed here in details.

2.3.1. Linear Sweep Voltammetry

Linear sweep voltammetry (LSV) is a common approach to determine the electrochemical window of the electrode-electrolyte systems. The potential applied to the electrode of interest is varied linearly with time under a constant scan rate (dV/dt) and the current as a function of potential is recorded.^[23] The typical LSV response curves of a capacitive electrode are shown in Figure 2. The upper curve is presented when the applied potential increases, and the lower one is drawn as the applied potential decreases. A plateau between V_{M-} and V_+ shows the capacitive behavior indicated by the constant current i_+/i_- .

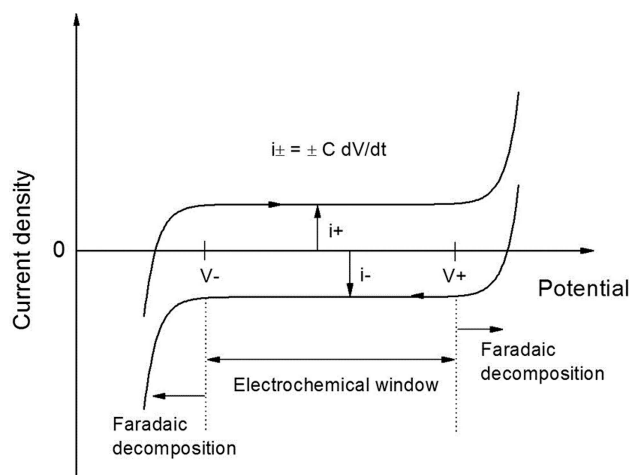


Figure 2. The typical LSV response curves of a capacitive electrode.

which is proportional to the capacitance C and the potential scan rate dV/dt . The substantial increase/decrease of the current above V_+ /below V_- is caused by the irreversible Faradaic reactions (e.g. decomposition of water). The capacitive potential window is therefore determined as $V_+ - V_-$.^[7]

While the LSV could be used to show the capacitive potential range of an electrode visually, a proper current density range and a cut-off current density should be used to determine V_- and V_+ . For example, for an electrochemical reaction with Butler-Volmer kinetics,^[25] the current as a function of the applied overpotential is plotted in Figure 3 with different current ranges. For a wider current range up to 500 mA shown in Figure 3a, the on-set overpotential could be visually determined as ~1.5 V. But for a narrower range up to 2 mA of the same curve (Figure 3b), the on-set overpotential could be ~0.9 V. Therefore, it is critical to specify the current range of interest and the current density (e.g. ±0.1 mA/cm²) used to determine the on-set potential.

In the case of supercapacitors, two factors should be considered for the determination of the cut-off current density. The first factor is the capacitive current proportional to the capacitance and the scan rate. A large charging/discharging current will be induced by the large capacitance of supercapacitor electrode. A very small scan rate (e.g. 1 mV/s) can reduce the influence of such current and is better for more accurate measure-

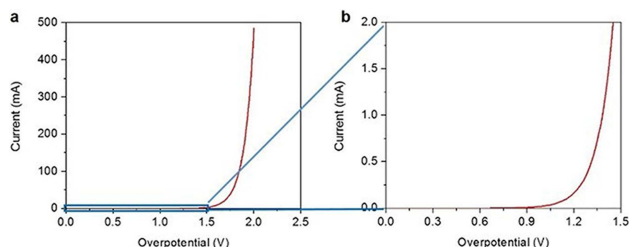


Figure 3. The current versus overpotential for an electrochemical reaction following the Butler-Volmer kinetics. (a) The current range of 0 to 500 mA; (b) the current range of 0 to 2 mA of the same experiment.

ments. The second one is the acceptable self-discharge current for a supercapacitor device. All electrochemical energy storage devices have certain amount of self-discharge or leakage current. A large self-discharge current is presented at high voltage for supercapacitors. Therefore, the operation voltage of a supercapacitor should be no more than the voltage with the maximum acceptable self-discharge current.

2.3.2. Galvanostatic Charge/Discharge

Instead of using dynamic measurements, steady-state measurements can avoid problems such as the difficulty to distinguish the reversible current from irreversible current. Galvanostatic charge/discharge is therefore used to determine the potential window.^[38–40] In such an approach, a constant current, usually the maximum acceptable self-discharge current, is applied to the electrode or cell until it comes to equilibrium. The potential of the electrode will increase/decrease due to the charge/discharge of the capacitance until the maximum/minimum value is reached. The applied current should be carefully chosen, as a high current density will result in a high working potential range. The test using a series of currents is recommended to compare the results with different work or application situations.

Galvanostatic charge/discharge has also been used to calculate coulombic efficiency to verify the proposed operation voltage of supercapacitor cells.^[28] A positive current is first applied to charge the supercapacitor from 0 V to the expected voltage, and then a negative current of the same magnitude is used to discharge the cell to 0 V. The ratio of the output of charge to the input of charge, calculated by the discharge time divided by the charge time, is the Coulombic efficiency of the supercapacitor device. The coulombic efficiency will become substantially low when the irreversible reactions happen in a considerable rate, resulting in an unbalanced charge and discharge time. High Coulombic efficiency (e.g. > 90%) implying good reversibility of the device is often used as a proof of the proper operation voltage. However, the selection of the charge/discharge current plays an important role, as a high current will result in a high Coulombic efficiency. The current range that best matches the practical application is recommended to be used for the tests.^[41] It should also be noted that the use of Coulombic efficiency to determine the potential range of a single electrode may not be meaningful, as the increase of potential means charging of a positive electrode but discharging of a negative electrode.

2.3.3. Impedance Spectroscopy

Electrochemical impedance spectroscopy (EIS) is frequently used to analyze the electrochemical processes in supercapacitors.^[7] The potentiostatic EIS applies a fixed direct current (DC) voltage plus a small alternating current (AC) voltage and measures the impedance of the system as a function of the AC frequency. The EIS reveals a lot of information of an electrochemical cell including impedances caused by capacitive, resistive, and diffusive behaviors. Several papers have reported that by setting the DC voltage

to be the voltage of interest, one can analyze the amount of non-capacitive behavior through potentiostatic EIS and determine whether the DC voltage is operational.^[42–44] A phase angle close to -90° at low AC frequencies indicates good capacitive behavior, but the value will shift at a high DC voltage due to irreversible electrochemical processes. As a result, the voltage range of a supercapacitor can be developed by using EIS.^[43] Specifically, EIS is conducted by increasing the DC voltage until the phase angle changes to a value (e.g. $> -80^\circ$) due to the irreversible processes and this DC voltage is considered as the maximum operational voltage. This approach could reveal irreversible processes that can't be easily identified in the LSV curves or the charge-discharge profiles.

3. Electrode-Aqueous Electrolyte Systems with High Working Voltage

The energy density, or more frequently reported specific energy in terms of Wh/kg, is the key factor that limits the application of supercapacitors. The working voltage range contributes more to the specific energy than the specific capacitance in capacitive energy storage simply because the energy is capacitance times voltage squared. Figure 4 plots the typical specific capacitance (F/g) versus potential range or cell voltage (V) for frequently reported electrode-electrolyte systems, with specific device energy (Wh/kg) calculated as a heat map. Region (1) of the map shows the typical performance of pseudo-capacitive/hybrid electrodes in aqueous electrolytes, which provide high specific capacitance (can be over 1000 F/g) but narrow potential range (0.6–1.4 V).^[8,36,45,46] Region (2) encompasses high-performance

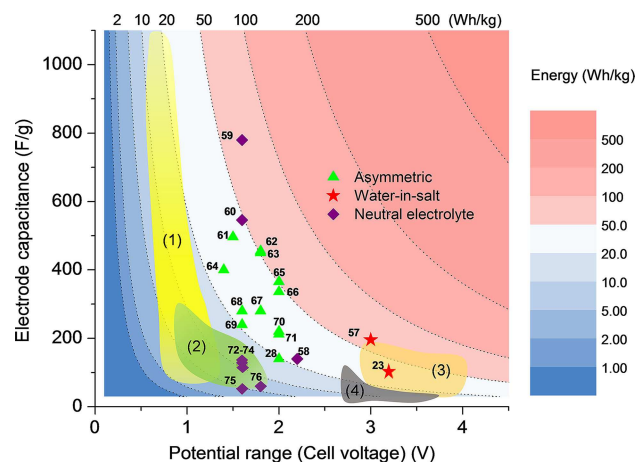


Figure 4. Heat map of specific energy calculated by specific capacitance versus potential range (cell voltage) for different electrode-electrolyte systems^[23,28,57–76]. The electrode capacitance (F/g) is either the value measured in a three-electrode system, or the one calculated from a two-electrode cell. For asymmetric system, the average capacitance of two electrodes is used. The specific energy of a supercapacitor cell (Wh/kg) is calculated by assuming two equal electrodes with equal capacitance connected in series. Four colored regions represent: (1) typical pseudo-capacitive/hybrid electrodes in aqueous electrolytes; (2) typical EDL electrodes in aqueous electrolytes; (3) typical electrodes in non-aqueous electrolytes; (4) commercially available supercapacitors.

EDL electrodes in aqueous electrolytes with considerable capacitance (less than 300 F/g), and slightly higher working potential than pseudocapacitive materials (0.8–1.8 V).^[47–50] It is clear that typical aqueous supercapacitors, even the ones with extremely high capacitances, have limited specific energy because of low working voltage range. When nonaqueous electrolytes are used, larger cell voltage, lower capacitance, and higher specific energy are resulted, as shown in region (3).^[49–51] At present, most commercial supercapacitor devices use the nonaqueous system for reasonable specific energy, plotted as region (4),^[52] but they are generally lower than those reported in the literature because of the inclusion of package weight.

To compete with nonaqueous devices and exploit the many advantages of aqueous electrolytes, a lot of research has been done to improve the working voltage range of aqueous systems for higher specific energy. Three major approaches are typically applied. The first approach relies on the asymmetric electrode design with positive and negative electrodes working in different potential ranges. Typical works plotted in Figure 4 show obvious improvements in specific energy as compared to those of symmetric aqueous supercapacitors.^[26,28,53–56] The second type uses high-concentration or “water-in-salt” electrolytes. They show great potential as their working voltage can be extended to over 3 V, as high as those used in the non-aqueous electrolytes.^[23,57] The third approach is to employ neutral electrolytes. Generally, large potential window and low capacitance systems are achieved by using neutral electrolytes instead of strong acids or alkalis.^[58] A slightly higher potential window can result in significant improvement of specific energy when the capacitance is high.^[59] The following sections show more details and discussions of the three approaches.

3.1. Asymmetric Electrodes

There are two typical types of electrode designs, as shown in Figures 5 and 6 and Table 1. The first type of electrode design uses different materials at the positive potential range (usually

pseudocapacitive or battery-like) and the negative potential range (usually carbon, can be pseudocapacitive or battery-like), respectively, as shown in Figure 5a.^[54,77] The different working potentials of positive and negative electrode result in the stretched working windows in the CV (Cyclic Voltammetry) plots as compared in Figures 5b–d.^[26] Using the activated carbon (AC) as the negative electrode, the AC/MnO₂ electrochemical capacitor (EC) system can improve the working potential voltage to 2 V in contrast to the symmetric MnO₂/MnO₂ system at 1 V. Using the AC/PbO₂ EC system, the voltage window can be increased further to 2.3 V. Other negative electrode materials have been investigated such as PEDOT^[28] while other positive electrode materials have been studied such as polypyrrole, anthraquinone on carbon and ... etc.^[26]

The second type of electrode design uses the same materials at the two electrodes.^[24,35,44,78] The voltage limit in the positive and negative operation range can be different due to the differences of the water hydrolysis potentials of the hydrogen evolution and oxygen evolution processes. The charge conservation of two electrodes results in:

$$Q = C_p U_p = C_N U_N, \quad (6)$$

Where Q is the total charge in the cell; C_p , C_N , U_p , and U_N are the specific capacitances, and the working potential ranges of the positive and negative electrodes, respectively. By changing the operation potentials of individual electrodes, C_p and C_N could modulate the U_p and U_N to fulfill the “waste” voltage potential range in the supercapacitor, as shown in Figure 6, where E_{V0} refers to the potential of both electrodes when the EC is fully discharged to 0 V.

3.2. High-Concentration Electrolytes

High-concentration electrolytes, including the water-in-salt type, can suppress water decomposition and improve the working voltage.^[20,21,38] “Water-in-salt” electrolyte refers to

Table 1. Supercapacitor with asymmetric electrodes in aqueous electrolytes *AC: Active Carbon; LDH: layered double hydroxide; CNF: carbon nanofiber; NW: nanowire.

Device configuration	Electrode		Electrolyte	Voltage	Energy Density (Wh kg ⁻¹)	Ref
	Anode	cathode		(V)		
Type I: electrodes with different materials	AC	CoNiFe-LDH/CNF	6 M KOH	1.6	30.2	[94]
	AC	PbO ₂	1 M H ₂ SO ₄	2.3	25	[26]
	PEDOT/CNT	MnO ₂ /CNT	2 M KNO ₃	1.8	13.5	[28]
	AC Nanofiber	MnO ₂ /graphene	Na ₂ SO ₄	1.8	51.1	[95]
	Graphene	CoNiS ₂ /graphene	1 M KOH	1.8	60	[96]
	S-VO _x -NWs carbon cloth	MnO ₂ /graphene	5 M LiCl	1.8	45	[97]
	Ppy/rGO	MnO ₂ /CNF on bacterial cellulose substrate	1.0 M Na ₂ SO ₄	2.0	32.9	[98]
Type II: electrodes with the same material but different mass	AC (mass ratio 2:3)		0.5 M Na ₂ SO ₄	2.0	16.2	[44]
	Pigment black (mass ratio 3:4)		0.3 M Na ₂ SO ₄	1.9	NA	[78]
	PAN-CNT (mass ratio 2:3)		K ₂ SO ₄	1.0 M HCl	NA	[35]
	AC (mass ratio 2:3)		0.5 M Na ₂ SO ₄	1.65	NA	[99]
			Na ₂ SO ₄	1.8	10.9	

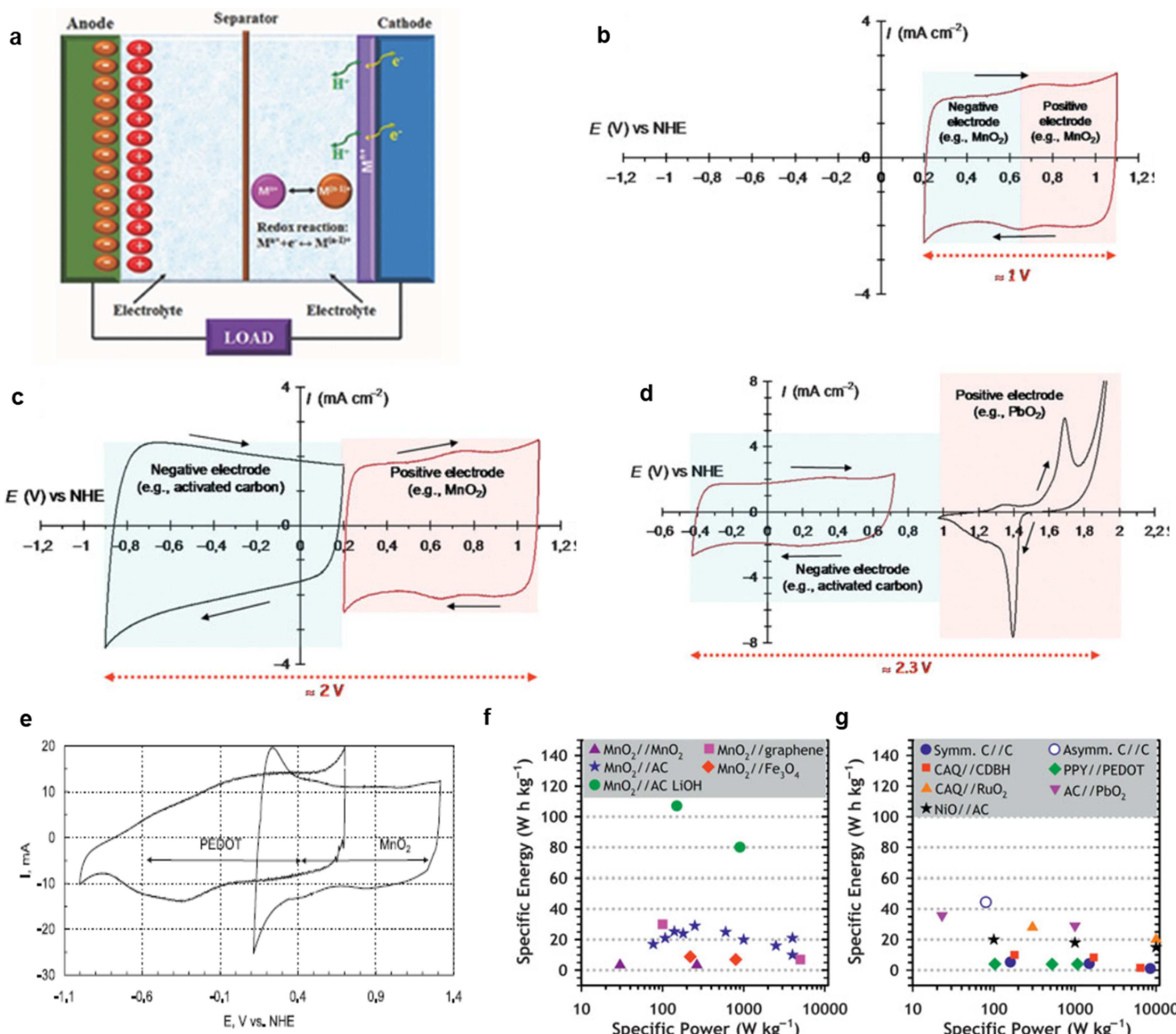


Figure 5. (a) The typical structure of asymmetric supercapacitors, Copyright 2017, Wiley-VCH.^[93] (b-d) The schematic plots of CV results for three aqueous-based electrochemical capacitors (ECs) in which the areas of potential window are shaded with different colors: red for the positive and blue for negative electrode, respectively. (b) symmetric MnO_2/MnO_2 EC with the α - MnO_2 electrodes in 0.5 M K_2SO_4 ; (c) asymmetric activated carbon/ MnO_2 EC in 0.5 M K_2SO_4 ; and (d) asymmetric activated carbon/ PbO_2 EC in 1 M H_2SO_4 . Copyright 2011, Cambridge Journals.^[26]

extremely high concentration, near saturated electrolyte, in which the “free” water molecule number is smaller than that of the solute molecule.^[79] Such electrolyte has been employed in high voltage aqueous lithium ion battery (LIB) (as shown in Figure 7a),^[80] and further extended to sodium ion battery,^[81] potassium ion battery,^[82] and magnesium ion battery.^[83] However, extending the electrolyte hydrolysis limit should combine with suitable electrode material for high voltage cells to extend the working potential window of electrolytes.^[51]

In a recent work,^[57] a two-step ALD/sulfurization process has been developed to deposit co-axial titanium disulfate (TiS_2) onto vertically aligned carbon nanotube forest (VACNT)^[84,85] as shown in Figure 7b. The TiS_2/CNT -LiTFSI (electrolyte) system can break the water electrolysis limit of 1.23 V and provides 195 F/g specific

capacitance, 60.9 Wh/kg energy density - highest among pseudocapacitors using metal oxides, conducting polymers, 2D transition metal carbides (MXENE) and other transition metal dichalcogenides as the electrode materials^[8,86-92] (Figures 7c,d). In general, the operation voltage is highly correlated to electrolyte concentration (Table 2, Figure 7a). The theoretical stable working potential window for the 21 m LiTFSI electrolyte is ~3 V for inert electrodes due to the effect of “depopulation of water”.^[51] With a relative inert VACNT frame network, the TiS_2 -VACNT can maintain the high electrochemical window (3 V) in the high concentration LiTFSI salt (21 m). Specifically, Table 2 shows that the high LiTFSI electrolyte concentration is found to extend the electrochemical potential working window for TiS_2/CNT electrodes from 1.9 V (1 m) to 3 V (21 m), while the high LiCl concentration can extend the window

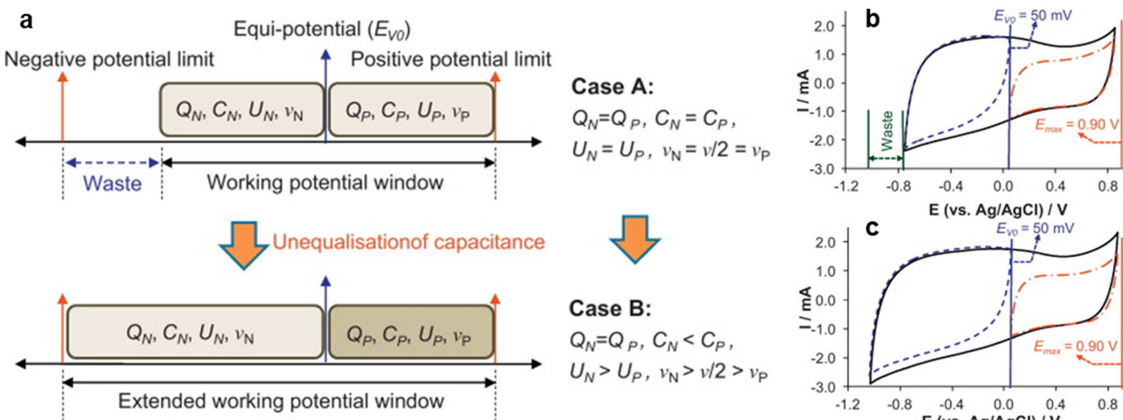


Figure 6. (a) Schematic diagram of a supercapacitor using the same material in both electrodes with the same specific capacitance (case A) and different specific capacitance (case B) in the positive and negative electrode to extend the working potential window, where v is the varying rate of the controlled cell voltage, or the responding electrode potential; the subscripts "P" and "N" indicate positive and negative electrodes, respectively. (b) (c) The example CVs using Monarch® 1300 (by Cabot Corp.) pigment black CMPB-PTFE (1.0 mg) in $0.3 \text{ mol L}^{-1} \text{ K}_2\text{SO}_4$. (b) The 1.6 V operational potential range following the construction of same working potential electrodes (Case A) and (c) The improved potential range of 1.90 V in accordance with the different electrode working potential (Case B).^[78] Copyright 2012, Elsevier Ltd.

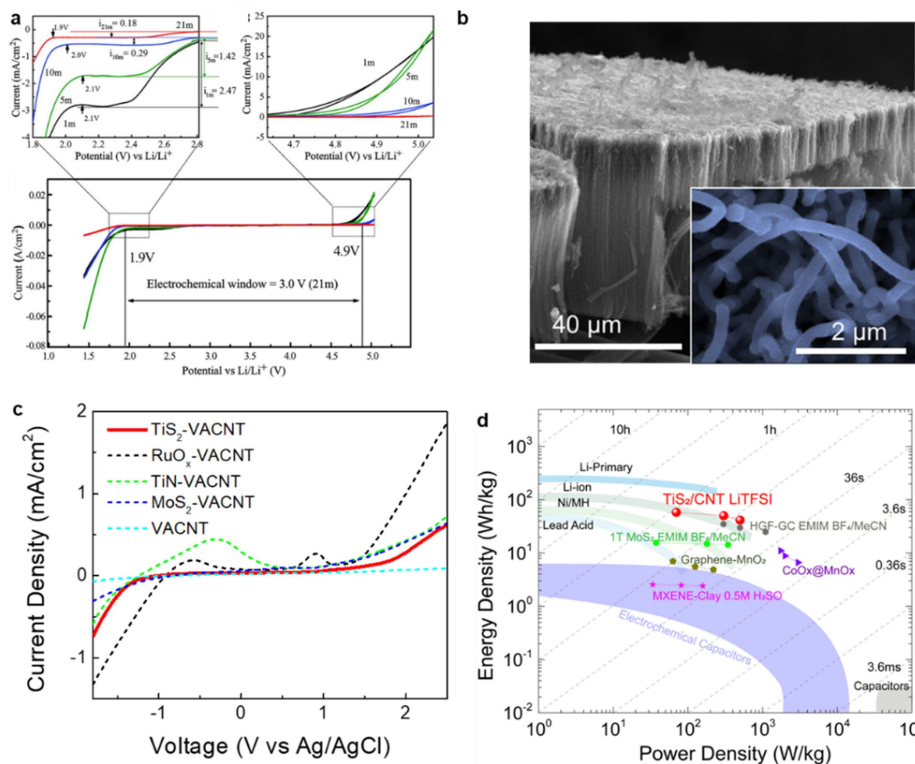


Figure 7. Extremely high concentration "water-in-salt" electrolyte for the high voltage supercapacitor using $\text{TiS}_2\text{-VACNT}$ as the electrode material. (a) The linear sweep voltammetry (LSV) results of the inert electrode in the 21 m LiTFSI electrolyte, with a scanning rate of 5 mV/s. (b) SEM image after a ALD TiN deposition process followed with a sulfurization step; (Inset) magnified SEM image showing individual electrodes with the diameter of $210 \pm 13 \text{ nm}$. (c) Linear sweep voltammetry (LSV) results of as-grown VACNT, TiS_2 composite-, RuO_x -, TiN -, and $\text{MoS}_2\text{-VACNT}$ electrodes in the 21 m LiTFSI electrolyte under a scan rate of 5 mV/s. Both TiS_2 composite-VACNT and pristine VACNT electrodes exhibit a 3 V stable operation window, while other electrodes have either broad redox peaks or hydrolysis reactions at a low voltage to reduce the electrochemical operation window. (d) Ragone plot for the state-of-art energy storage systems showing $\text{TiS}_2\text{-VACNT}$ composite with the highest energy density among various families of non-carbon materials, including metal oxides, metal chalcogenides, and metal carbide-based systems.^[86-92] Copyright 2018, Wiley.

for $\text{TiS}_2\text{/CNT}$ electrodes from 1.4 V (1 m) to 2.35 V (20 m). Furthermore, the large TFSI anion concentration can form a higher Helmholtz layer potential to increase the threshold of oxygen

evolution swing at 1.7 V than that of the high Cl anions at 1.05 V. Electrolytes based on H_2SO_4 and NaCl have either H^+ or Na^+ ions, which won't intercalate with TiS_2 . In fact, H^+ ions increase the

Table 2. TiS_2/CNT electrodes in electrolytes with different solvent, solute and concentration^[57]. NMP is abbreviation for N-Methyl-2-pyrrolidone.
Copyright 2018, Wiley.

Voltage vs Ag/AgCl	Min voltage	Max voltage	Voltage window	Capacitance F/g (10 mV/s)
0.5 M H_2SO_4	-0.2	1.0	1.2	10.4
1 m NaCl	-0.4	0.1	0.5	0.2
1 m LiCl	-0.4	1.0	1.4	18.75
10 m LiCl	-0.5	1	1.5	30
20 m LiCl	-1.3	1.05	2.35	80
1 m LiTFSI	-0.8	1.1	1.9	86
10 m LiTFSI	-1	1.2	2.3	102
20 m LiTFSI	-1.3	1.7	3	120
Voltage vs Ag/Ag + Organic	Min voltage	Max voltage	Voltage window	Capacitance F/g (10 mV/s)
1 m LiTFSI in NMP	-1.5	0.9	2.4	31.25

probability of hydrogen evolution by lowering the overpotential voltage in the hydrogen evolution reaction (HER) which decreases the electrochemical voltage window.

The intercalation voltage for TiS_2 is reduced to ~ 2 V vs Li/Li $+$ (-1.05 vs RHE, -1.24 V Ag/AgCl) which is above its water hydrolysis voltage around -1.4 V vs Ag/AgCl (1.9 V vs Li/Li $+$). As shown in Figure 6c, many of the other high capacitance materials are not suitable to fully utilize the 3 V voltage window with the 21 m LiTFSI electrolyte. The RuO_x -VACNT electrode system has a high redox peak but it can catalyze the hydrogen evolution and oxygen evolution processes to decrease the stable operation voltage window.^[100] The TiN-VACNT electrode shows the undesirable broad and high electrochemical peak near -0.4 V which could be induced by the hydrolysis process and the TiN-TiO_2 impurity transition reactions due to the instability of TiN in acid media.^[101] The MoS_2 -VACNT system, on the other hand, has the catalytic reactions of HER and oxygen evolution (OER),^[102] such that its electrochemical voltage window in the 21 m LiTFSI electrode decreases due to the low overpotential from the water hydrolysis process.

Furthermore, the high LiTFSI concentration electrolyte can increase the conductivity of ions and lower the electrolyte impedance^[103] to improve the power density performances of energy storage systems. On the other hand, increasing the concentration of the electrolyte could potentially extend the working temperature due to the freezing temperature depression effect.^[104] Incorporating temperature resilient materials, the supercapacitor cell using the 21 m LiTFSI/PVA/ H_2O electrolyte was shown to work from -50°C to 300°C .^[105] The freezing point of water in such high concentration electrolyte can be suppressed from the typical 0°C to -74°C . However, the “frozen” electrolyte provide poor ionic conductivity such that the capacitor only maintains about $>50\%$ of its room-temperature capacitance at -50°C .^[105]

3.3. Neutral Electrolytes

In general, electrodes will have different working potential ranges in electrolytes with different pH levels, including acidic, alkaline, and neutral electrolytes.^[58,112,113] Neutral electrolytes could result in high operation voltages as compared with those in acidic and alkaline electrolytes by reducing the possibility of inducing the water hydrolysis reaction due to either the hydrogen evolution reaction (HER) or oxygen evolution reaction (OER).^[58,112,113] Furthermore, materials with low absorption energy of hydrogen or oxygen are generally good catalysts for HER and OER.^[114] Meanwhile, materials with poor catalytic efficiency such as carbon-based materials have high overpotentials. Using chemically stable, activated carbon as the electrodes, the capacitance is mainly dominated by the EDL capacitance and is highly dependent on the ion shapes, ion-ion interactions, and diffusion coefficients in the electrolytes.^[115] For example, the EDL capacitance in different electrolytes in Figure 8 is related to the ionic mobility in the order of hydrated ion size: $\text{Li}^+ < \text{Na}^+ < \text{K}^+$. Unlike the pseudocapacitive system,^[110] fast transfer of ions into the electrode/electrolyte interface is needed for quick redox processes, while simple charging and discharging of the EDLCs does not require very high ion mobility. The porous structure of the electrode is already saturated with ions located on electrode/electrolyte interface, and they are pushed off from the electrode with a small distance. Hence, high mobility ions might migrate too fast and aggravate the efficient charge propagation.^[58] In comparison, a pseudocapacitive system with electrodes made of AC and MnO_2 shows specific capacitance in neutral electrolyte in order of $\text{K}_2\text{SO}_4 < \text{Na}_2\text{SO}_4 < \text{Li}_2\text{SO}_4$ at low scan rates, while the reverse at high scan rates.^[110]

In neutral electrolytes, the overpotential of hydrogen evolution could easily reach 200 mV,^[116] and the over potential for oxygen evolution^[117] could extend to 1.8 V and above (Table 3).^[118,119] Furthermore, some very highly capacitive materials are also outstanding catalysts for water which can result in low voltage operation to decrease the energy density. As discussed in the previous section, MoS_2 from the transition metal dichalcogenide family (TMDC) is a material with high energy storage capacity,^[120,121] yet the nanocrystalline MoS_2 could provide exceptional low overpotential 40~50 mV in acid environmental which results in a narrow operational window.^[122,123] However, in neutral or base electrolytes, MoS_2 based supercapacitor could perform better with high working voltages and high capacitances.^[86,124,125] Similarly, IrO_2 and RuO_2 have low oxygen evolution overpotentials,^[126] which are not desirabale in base electrolyte cells.^[75,127,128] By suppressing the water hydrolysis process with surface redox reactions in neutral electrolyte, a recent report of nanoengineered Ni–O–Mn electrode can operate up to 2.4 Volts.^[129]

As show in Table 2, electrolytes made of 1 m LiTFSI dissolved in NMP shows a wider operational voltage range than that of electrolyte made of 1 m LiTFSI in H_2O . However, organic solvents have lower ionic conductivity for the carrier transfer process at the interface to result in higher impedances and lower capacitances.^[130–132] Although electrolytes based on

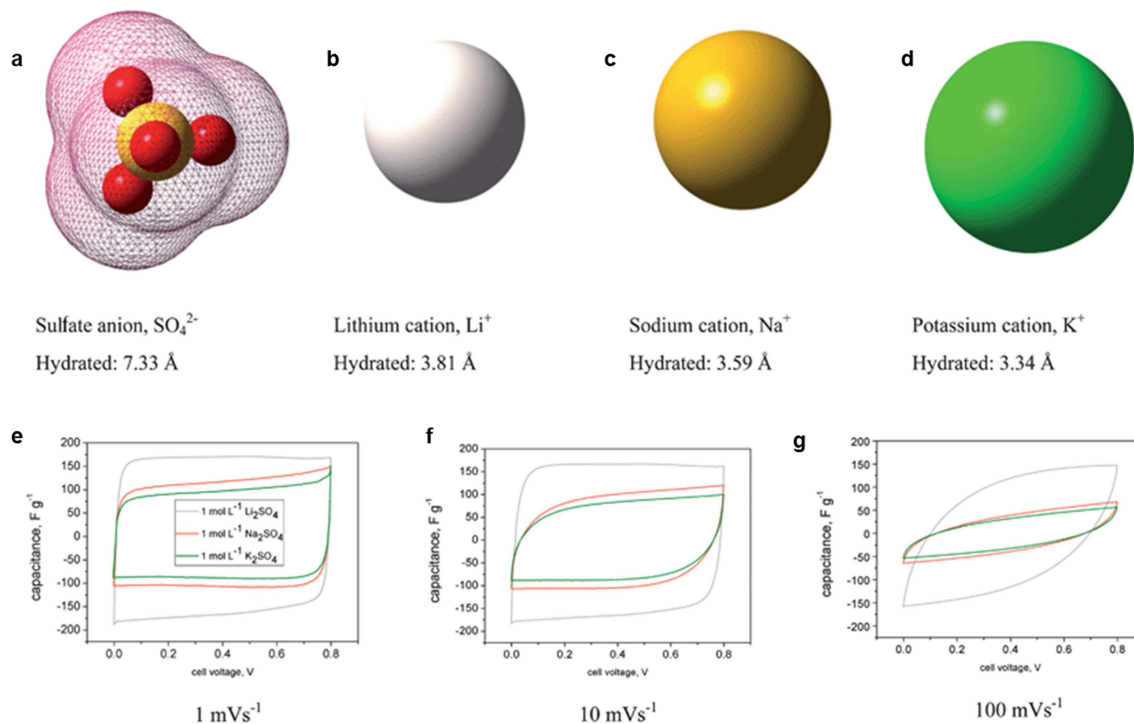


Figure 8. (a–d) Ion shape and dimensions in aqueous solutions. The scale between the pictures is not preserved; the mesh around the sulfate anion in (a) represents the molecular orbitals. (e–g) Cyclic voltammograms at different scan rates (1, 10 and 100 mVs⁻¹, respectively) with current values recalculated to capacitance for carbon–carbon capacitor operating in 1 mol L⁻¹ alkali metal (Li, Na, K) sulfate solutions.^[58] Copyright, 2012 RSC publishing group.

Table 3. Summary of high operational voltage enabled by electrolyte. * m: molal, mol/kg of solvent; M: mol/L.

Electrolyte type	Electrolyte Type	Concentration	Electrode Anode	Cathode	Voltage (V)	Energy Density (Wh kg ⁻¹)	Ref
High concentration	LiTFSI	21 m	TiS ₂ /CNT		3.0	60.9	[57]
	LiTFSI	21 m	AC		2.9	12.5	[106]
	LiTFSI	31.3 m	AC/CB/PTFE		2.4	30.4	[107]
	KCH ₃ COO	7.6 m	AC		2.0	19.8	[108]
	Mg(CH ₃ COO) ₂	1 M	Mo ₂ C		2.4	20	[109]
	Li ₂ SO ₄	1 m	AC/PVDF/CB		2.2	NA	[58]
	K ₂ SO ₄	1 m	AC	MnO ₂	1.8	17	[110]
	Li ₂ SO ₄	1 M	Ti ₂ CT _x (MXene)		1.5	20.1	[111]
Neutral electrolyte	Na ₂ SO ₄	0.5 M	Seaweed carbons		1.6	10.8 Wh	[73]

organic solvent can provide up to 4.2 V of working potential range,^[133,134] supercapacitors using such electrolytes result in lower energy density.^[135] Thus, aqueous electrolyte could be suitable for high voltage and high energy density supercapacitors (Table 3).

4. Summary and Outlook

High concentration and neutral pH electrolytes have been discussed in this work for high-voltage supercapacitors based on aqueous electrolytes. High concentration electrolytes such as Li based water-in-salt electrolytes have higher price than those of other electrolytes in the TFSI family such as KTFSI, NaTFSI and Al(TFSI)₃.^[136] Furthermore, the developments of electrolyte with large anion, high solubility, and cation mobility in water are good future directions. There are also many

possible approaches to increase the operating potential windows of supercapacitors, such as the application of isotope D₂O and D₃PO₄^[137] and ions with higher charges such as Mg²⁺, Ca²⁺ and Zn²⁺ as electrolytes.^[138] In the area of neutral pH aqueous Mg²⁺ electrolytes, including MgSO₄ and MgCl₂, stable electrodes materials could achieve voltage windows > 2 V and capacitance > 100 F/g.^[109] In principle, choosing the feasible pseudocapacitance materials in suitable electrolytes and constructing electrodes with high surface area are the key elements to increase the EDL capacitance and pseudocapacitance and high voltage operation windows can result in the high energy storage density. Furthermore, aqueous electrolytes with asymmetric electrodes design can improve the performances of supercapacitors with both high voltage and high energy density as well as good safety and low cost.^[26,55,110] However, high voltage operations could also cause the voltage drop and leaking current phenomena which are not desirable in practical

applications.^[139] These and other issues as well as further enhancing the energy storage performances of supercapacitors are topics to be continuously investigated and improved.

Acknowledgements

Author X. Z and C. S. Contribute equally to this paper.

Conflict of Interest

The authors declare no conflict of interest.

Keywords: aqueous electrolyte • high concentration electrolyte • high voltage • supercapacitors • symmetric/asymmetric capacitors

- [1] D. Shin, C. Shen, M. Sanghadasa, L. Lin, *Adv. Mater. Tech.* **2018**, 1800209.
- [2] C. W. Shen, Y. X. Xie, M. Sanghadasa, Y. Tang, L. S. Lu, L. Lin, *ACS Appl. Mater. Interfaces* **2017**, 9, 39391–39398.
- [3] M. Armand, J. M. Tarascon, *Nature* **2008**, 451, 652–657.
- [4] J. R. Miller, *J. Power Sources* **2016**, 326, 726–735.
- [5] A. Burke, *Electrochim. Acta* **2007**, 53, 1083–1091.
- [6] J. R. Miller, P. Simon, *Science* **2008**, 321, 651–652.
- [7] B. E. Conway, *Electrochemical Supercapacitors*. Springer US: Boston, MA, 1999.
- [8] P. Simon, Y. Gogotsi, *Nat. Mater.* **2008**, 7, 845–854.
- [9] C. Shen, S. Xu, Y. Xie, M. Sanghadasa, X. Wang, L. Lin, *J. Microelectromech. Syst.* **2017**, 26, 949–965, DOI: 10.1109/JMEMS.2017.2723018
- [10] Z. L. Wang, *Adv. Funct. Mater.* **2008**, 18, 3553–3567.
- [11] Y. Zhang, H. Yang, *J. Power Sources* **2011**, 196, 4128–4135.
- [12] I. Hadjipaschalidis, A. Poulikkas, V. Efthimiou, *Renewable Sustainable Energy Rev.* **2009**, 13, 1513–1522.
- [13] X. Zang, C. Shen, Y. Chu, B. Li, M. Wei, J. Zhong, M. Sanghadasa, L. Lin, *Adv. Mater.* **2018**, 30, 1800062.
- [14] C. Shen, Y. Xie, B. Zhu, M. Sanghadasa, Y. Tang, L. Lin, *Sci. Rep.* **2017**, 7, 14324.
- [15] C. Shen, C. Wang, M. Sanghadasa, L. Lin, *RSC Adv.* **2017**, 7, 11724–11731.
- [16] D. Yu, Q. Qian, L. Wei, W. Jiang, K. Goh, J. Wei, J. Zhang, Y. Chen, *Chem. Soc. Rev.* **2015**, 44, 647–662.
- [17] I. Gradzka, M. Gierszewski, J. Karolczak, M. Ziolek, *Phys. Chem. Chem. Phys.* **2018**, 20, 7710–7720.
- [18] Y. Wang, W. H. Zhong, *ChemElectroChem* **2015**, 2, 22–36.
- [19] M. Ciobanu, J. P. Wilburn, M. L. Krim, D. E. Cliffel, *Fundamentals*, Elsevier, 2007, pp 3–29.
- [20] E. Roduner, *Catal. Today* **2018**, 309, 263–268.
- [21] X. Zou, Y. Zhang, *Chem. Soc. Rev.* **2015**, 44, 5148–5180.
- [22] L. M. Suo, O. Borodin, T. Gao, M. Olguin, J. Ho, X. L. Fan, C. Luo, C. S. Wang, K. Xu, *Science* **2015**, 350, 938–943.
- [23] H. Tomiyasu, H. Shikata, K. Takao, N. Asanuma, S. Taruta, Y.-Y. Park, *Sci. Rep.* **2017**, 7, 45048–45048.
- [24] Z. Dai, C. Peng, J. H. Chae, K. C. Ng, G. Z. Chen, *Sci. Rep.* **2015**, 5, 9854–9854.
- [25] A. J. Bard, L. R. Faulkner, *Electrochemical methods: Fundamentals and applications*. JOHN WILEY & SONS, INC., 2001.
- [26] J. W. Long, D. Bélanger, T. Brousse, W. Sugimoto, M. B. Sassin, O. Crosnier, *MRS Bull.* **2011**, 36, 513–522.
- [27] V. Khomenko, E. Raymundo-Piñero, E. Frackowiak, F. Béguin, *Appl. Phys. A* **2006**, 82, 567–573.
- [28] V. Khomenko, E. Raymundo-Piñero, F. Béguin, *J. Power Sources* **2006**, 153, 183–190.
- [29] M. Seredych, D. Hulicova-Jurcakova, G. Q. Lu, T. J. Bandosz, *Carbon* **2008**, 46, 1475–1488.
- [30] Y. Shao, G. Yin, J. Zhang, Y. Gao, *Electrochim. Acta* **2006**, 51, 5853–5857.
- [31] F. Shi, L. Li, X.-L. Wang, C.-D. Gu, J.-P. Tu, *RSC Adv.* **2014**, 4, 41910–41921.
- [32] M. Ghidiu, M. R. Lukatskaya, M.-Q. Zhao, Y. Gogotsi, M. W. Barsoum, *Nature* **2014**, 516, 78–81.
- [33] Y. Xia, T. S. Mathis, M.-Q. Zhao, B. Anasori, A. Dang, Z. Zhou, H. Cho, Y. Gogotsi, S. Yang, *Nature* **2018**, 557, 409–412.
- [34] B. Anasori, M. R. Lukatskaya, Y. Gogotsi, *Nat. Rev. Mater.* **2017**, 2, 16098–16098.
- [35] C. Peng, S. Zhang, D. Jewell, G. Z. Chen, *Prog. Nat. Sci.* **2008**, 18, 777–788.
- [36] G. A. Snook, P. Kao, A. S. Best, *J. Power Sources* **2011**, 196, 1–12.
- [37] R. Warren, F. Sammoura, K. S. Teh, A. Kozinda, X. Zang, L. Lin, *Sens. Actuators A* **2015**, 231, 65–73.
- [38] C. Wessells, R. Ruffo, R. A. Huggins, Y. Cui, *Electrochim. Solid-State Lett.* **2010**, 13, A59–A59.
- [39] C. Wessells, R. A. Huggins, Y. Cui, *J. Power Sources* **2011**, 196, 2884–2888.
- [40] S. F. Lux, L. Terborg, O. Hachmoller, T. Placke, H. W. Meyer, S. Passerini, M. Winter, S. Nowak, *J. Electrochim. Soc.* **2013**, 160, A1694–A1700.
- [41] M. D. Stoller, R. S. Ruoff, *Energy Environ. Sci.* **2010**, 3, 1294–1294.
- [42] H.-H. Shen, C.-C. Hu, *J. Electroanal. Chem.* **2016**, 779, 161–168.
- [43] T.-H. Wu, Y.-H. Chu, C.-C. Hu, L. J. Hardwick, *Electrochim. Commun.* **2013**, 27, 81–84.
- [44] T.-H. Wu, C.-T. Hsu, C.-C. Hu, L. J. Hardwick, *J. Power Sources* **2013**, 242, 289–298.
- [45] A. Eftekhari, L. Li, Y. Yang, *J. Power Sources* **2017**, 347, 86–107.
- [46] Q. Meng, K. Cai, Y. Chen, L. Chen, *Nano Energy* **2017**, 36, 268–285.
- [47] X. Fan, X. Chen, L. Dai, *Curr. Opin. Colloid Interface Sci.* **2015**, 20, 429–438.
- [48] W. Lv, Z. Li, Y. Deng, Q.-H. Yang, F. Kang, *Energy Storage Mater.* **2016**, 2, 107–138.
- [49] X. Li, B. Wei, *Nano Energy* **2013**, 2, 159–173.
- [50] W. Yang, M. Ni, X. Ren, Y. Tian, N. Li, Y. Su, X. Zhang, *Curr. Opin. Colloid Interface Sci.* **2015**, 20, 416–428.
- [51] C. Zhong, Y. Deng, W. Hu, J. Qiao, L. Zhang, J. Zhang, *Chem. Soc. Rev.* **2015**, 44, 7484–7539.
- [52] A. Burke, H. Zhao, *Present and Future Applications of Supercapacitors in Electric and Hybrid Vehicles*, 2015/09//: IEEE, p. 1–5.
- [53] Y. Huang, Y. Zeng, M. Yu, P. Liu, Y. Tong, F. Cheng, X. Lu, *Small Methods* **2018**, 2, 1700230–1700230.
- [54] J. Sun, C. Wu, X. Sun, H. Hu, C. Zhi, L. Hou, C. Yuan, *J. Mater. Chem. A* **2017**, 5, 9443–9464.
- [55] M. Rajkumar, C.-T. Hsu, T.-H. Wu, M.-G. Chen, C.-C. Hu, *Prog. Nat. Sci.* **2015**, 25, 527–544.
- [56] S. Zheng, Z.-S. Wu, S. Wang, H. Xiao, F. Zhou, C. Sun, X. Bao, H.-M. Cheng, *Energy Storage Mater.* **2017**, 6, 70–97.
- [57] X. Zang, C. Shen, E. Kao, R. Warren, R. Zhang, K. S. Teh, J. Zhong, M. Wei, B. Li, Y. Chu, M. Sanghadasa, A. Schwartzberg, L. Lin, *Adv. Mater.* **2018**, 30, 1704754.
- [58] K. Fic, G. Lota, M. Meller, E. Frackowiak, *Energy Environ. Sci.* **2012**, 5, 5842–5850.
- [59] T. Lin, I. W. Chen, F. Liu, C. Yang, H. Bi, F. Xu, F. Huang, *Science* **2015**, 350, 1508–1513.
- [60] S. Dhibar, P. Bhattacharya, G. Hatui, S. Sahoo, C. K. Das, *ACS Sustainable Chem. Eng.* **2014**, 2, 1114–1127.
- [61] J. Xiao, S. Yang, *J. Mater. Chem.* **2012**, 22, 12253–12253.
- [62] Z. Fan, J. Yan, T. Wei, L. Zhi, G. Ning, T. Li, F. Wei, *Adv. Funct. Mater.* **2011**, 21, 2366–2375.
- [63] Y. Shao, H. Wang, Q. Zhang, Y. Li, *J. Mater. Chem. C* **2013**, 1, 1245–1251.
- [64] J. Zhang, J. Jiang, H. Li, X. S. Zhao, *Energy Environ. Sci.* **2011**, 4, 4009–4009.
- [65] Y. Zhao, W. Ran, J. He, Y. Huang, Z. Liu, W. Liu, Y. Tang, L. Zhang, D. Gao, F. Gao, *Small* **2015**, 11, 1310–1319.
- [66] Y. Jin, H. Chen, M. Chen, N. Liu, Q. Li, *ACS Appl. Mater. Interfaces* **2013**, 5, 3408–3416.
- [67] C. J. Jafta, F. Nkosi, L. Le Roux, M. K. Mathe, M. Kebede, K. Makgopa, Y. Song, D. Tong, M. Oyama, N. Manyala, S. Chen, K. I. Ozoemena, *Electrochim. Acta* **2013**, 110, 228–233.
- [68] H. Xia, C. Hong, B. Li, B. Zhao, Z. Lin, M. Zheng, S. V. Savilov, S. M. Aldoshin, *Adv. Funct. Mater.* **2015**, 25, 627–635.
- [69] Z.-S. Wu, W. Ren, D.-W. Wang, F. Li, B. Liu, H.-M. Cheng, *ACS Nano* **2010**, 4, 5835–5842.

- [70] M. Liu, W. W. Tjiu, J. Pan, C. Zhang, W. Gao, T. Liu, *Nanoscale* **2014**, *6*, 4233–4233.
- [71] L.-Q. Fan, G.-J. Liu, J.-H. Wu, L. Liu, J.-M. Lin, Y.-L. Wei, *Electrochim. Acta* **2014**, *137*, 26–33.
- [72] Q. Abbas, D. Pajak, E. Frackowiak, F. Béguin, *Electrochim. Acta* **2014**, *140*, 132–138.
- [73] M. P. Bichat, E. Raymundo-Pinero, F. Beguin, *Carbon* **2010**, *48*, 4351–4361.
- [74] L. Demarconnay, E. Raymundo-Piñero, F. Béguin, *Electrochim. Commun.* **2010**, *12*, 1275–1278.
- [75] H. Xia, Y. S. Meng, G. L. Yuan, C. Cui, L. Luc, *Electrochim. Solid-State Lett.* **2012**, *15*, A60–A63.
- [76] D. Jiménez-Cordero, F. Heras, M. A. Gilarranz, E. Raymundo-Piñero, *Carbon* **2014**, *71*, 127–138.
- [77] P. Przygocki, Q. Abbas, F. Béguin, *Electrochim. Acta* **2018**, *269*, 640–648.
- [78] J. H. Chae, G. Z. Chen, *Electrochim. Acta* **2012**, *86*, 248–254.
- [79] W. Sun, L. M. Suo, F. Wang, N. Eidson, C. Y. Yang, F. D. Han, Z. H. Ma, T. Gao, M. Zhu, C. S. Wang, *Electrochim. Commun.* **2017**, *82*, 71–74.
- [80] L. Smith, B. Dunn, *Science* **2015**, *350*, 918–918.
- [81] L. Suo, O. Borodin, Y. Wang, X. Rong, W. Sun, X. Fan, S. Xu, M. A. Schroeder, A. V. Cresce, F. Wang, C. Yang, Y.-S. Hu, K. Xu, C. Wang, *Adv. Energy Mater.* **2017**, *7*, 1701189.
- [82] D. P. Leonard, Z. X. Wei, G. Chen, F. Du, X. L. Ji, *ACS Energy Lett.* **2018**, *3*, 373–++.
- [83] F. Wang, X. L. Fan, T. Gao, W. Sun, Z. H. Ma, C. Y. Yang, F. Han, K. Xu, C. S. Wang, *ACS Cent. Sci.* **2017**, *3*, 1121–1128.
- [84] Y. Jiang, P. Wang, X. Zang, Y. Yang, A. Kozinda, L. Lin, *Nano Lett.* **2013**, *13*, 3524–3530.
- [85] R. Warren, F. Sammoura, F. Tounsi, M. Sanghadasa, L. Lin, *J. Mater. Chem. A* **2015**, *3*, 15568–15575.
- [86] M. Acerce, D. Voiry, M. Chhowalla, *Nat. Nanotechnol.* **2015**, *10*, 313–318.
- [87] M. Ghidiu, M. R. Lukatskaya, M. Q. Zhao, Y. Gogotsi, M. W. Barsoum, *Nature* **2014**, *516*, 78–81.
- [88] J. P. Liu, J. Jiang, C. W. Cheng, H. X. Li, J. X. Zhang, H. Gong, H. J. Fan, *Adv. Mater.* **2011**, *23*, 2076–++.
- [89] G. H. Yu, L. B. Hu, M. Vosgueritchian, H. L. Wang, X. Xie, J. R. McDonough, X. Cui, Y. Cui, Z. N. Bao, *Nano Lett.* **2011**, *11*, 2905–2911.
- [90] Y. X. Xu, Z. Y. Lin, X. Zhong, X. Q. Huang, N. O. Weiss, Y. Huang, X. F. Duan, *Nat. Commun.* **2014**, *5*.
- [91] C. C. Hu, K. H. Chang, M. C. Lin, Y. T. Wu, *Nano Lett.* **2006**, *6*, 2690–2695.
- [92] M. Toupin, T. Brousse, D. Belanger, *Chem. Mater.* **2004**, *16*, 3184–3190.
- [93] N. Choudhary, C. Li, J. Moore, N. Nagaiah, L. Zhai, Y. Jung, J. Thomas, *Adv. Mater.* **2017**, *29*, 1605336–1605336.
- [94] F. Wang, S. Sun, Y. Xu, T. Wang, R. Yu, H. Li, *Sci. Rep.* **2017**, *7*, 4707.
- [95] Z. J. Fan, J. Yan, T. Wei, L. J. Zhi, G. Q. Ning, T. Y. Li, F. Wei, *Adv. Funct. Mater.* **2011**, *21*, 2366–2375.
- [96] W. Chen, C. Xia, H. N. Alshareef, *ACS Nano* **2014**, *8*, 9531–9541.
- [97] T. Zhai, X. H. Lu, Y. C. Ling, M. H. Yu, G. M. Wang, T. Y. Liu, C. L. Liang, Y. X. Tong, Y. Li, *Adv. Mater.* **2014**, *26*, 5869–5875.
- [98] L. F. Chen, Z. H. Huang, H. W. Liang, Q. F. Guan, S. H. Yu, *Adv. Mater.* **2013**, *25*, 4746–4752.
- [99] I. Pineiro-Prado, D. Salinas-Torres, R. Ruiz-Rosas, E. Morallón, D. Cazorla-Amorós, *Front. Mater.* **2016**, *3*.
- [100] S. D. Tilley, M. Schreier, J. Azevedo, M. Stefkík, M. Graetzel, *Adv. Funct. Mater.* **2014**, *24*, 303–311.
- [101] Y. J. Han, X. Yue, Y. S. Jin, X. D. Huang, P. K. Shen, *J. Mater. Chem. A* **2016**, *4*, 3673–3677.
- [102] D. H. Deng, K. S. Novoselov, Q. Fu, N. F. Zheng, Z. Q. Tian, X. H. Bao, *Nat. Nanotechnol.* **2016**, *11*, 218–230.
- [103] M. Lovric, M. Hermes, F. Scholz, *J. Solid State Electrochem.* **1998**, *2*, 401–404.
- [104] J. W. Mellor, *Modern inorganic chemistry*. Longmans, Green, 1912.
- [105] M. S. Wei, B. X. Li, X. N. Zang, W. S. Chen, Y. Chu, M. Sanghadasa, L. W. Lin, Flexible Harsh Environment Micro Supercapacitors Using Direct-Write 2d Transition Metal Carbides, 2017 19th International Conference on Solid-State Sensors, Actuators and Microsystems (Transducers); **2017**, pp. 702–705.
- [106] N. Kumar Thangavel, K. Mahankali, Y. Ding, L. Arava, Water-in-Salt Electrolytes for High-Voltage Supercapacitors. Meeting Abstracts, **2018**, *The Electrochemical Society*; **2018**, p. 148–148.
- [107] P. Lannelongue, R. Bouchal, E. Mourad, C. Bodin, M. Olarte, S. Le Vot, F. Favier, O. Fontaine, *J. Electrochem. Soc.* **2018**, *165*, A657–A663.
- [108] Z. Y. Tian, W. J. Deng, X. S. Wang, C. Y. Liu, C. Li, J. T. Chen, M. Q. Xue, R. Li, F. Pan, *Funct. Mater. Lett.* **2017**, *10*.
- [109] X. Zang, L. Lin, M. Sanghadasa, Nanostructured Carbide Materials Enable High Performance Pseudocapacitors in Mg-Ion Electrolytes. 48th Power Sources Conference; **2018**, Denver; **2018**.
- [110] Q. T. Qu, P. Zhang, B. Wang, Y. H. Chen, S. Tian, Y. P. Wu, R. Holze, *J. Phys. Chem. C* **2009**, *113*, 14020–14027.
- [111] S. A. Melchior, K. Raju, I. S. Ike, R. M. Erasmus, G. Kabongo, I. Sigalas, S. E. Iyuke, K. I. Ozoemena, *J. Electrochem. Soc.* **2018**, *165*, A501–A511.
- [112] D. Friebel, P. Broekmann, K. Wandelt, *Phys. Status Solidi A* **2004**, *201*, 861–869.
- [113] E. Frackowiak, M. Meller, J. Menzel, D. Gastol, K. Fic, *Faraday Discuss.* **2014**, *172*, 179–198.
- [114] X. Zang, W. Chen, X. Zou, J. N. Hohman, L. Yang, B. Li, M. Wei, C. Zhu, J. Liang, M. Sanghadasa, J. Gu, L. Lin, *Adv. Mater.* **2018**, 1805188.
- [115] B. Gao, Z. F. Liu, *J. Chem. Phys.* **2004**, *121*, 8299–8306.
- [116] M. G. Walter, E. L. Warren, J. R. McKone, S. W. Boettcher, Q. X. Mi, E. A. Santori, N. S. Lewis, *Chem. Rev.* **2010**, *110*, 6446–6473.
- [117] J. K. Norskov, T. Bligaard, J. Rossmeisl, C. H. Christensen, *Nat. Chem.* **2009**, *1*, 37–46.
- [118] N. Batisse, E. Raymundo-Pinero, *J. Power Sources* **2017**, *348*, 168–174.
- [119] X. W. Yang, Y. S. He, G. P. Jiang, X. Z. Liao, Z. F. Ma, *Electrochim. Commun.* **2011**, *13*, 1166–1169.
- [120] T. Stephenson, Z. Li, B. Olsen, D. Mitlin, *Energy Environ. Sci.* **2014**, *7*, 209–231.
- [121] X. Y. Chia, A. Y. S. Eng, A. Ambrosi, S. M. Tan, M. Pumera, *Chem. Rev.* **2015**, *115*, 11941–11966.
- [122] W. S. Chen, J. J. Gu, Q. L. Liu, R. C. Luo, L. L. Yao, B. Y. Sun, W. Zhang, H. L. Su, B. Chen, P. Liu, D. Zhang, *ACS Nano* **2018**, *12*, 308–316.
- [123] D. S. Kong, H. T. Wang, J. J. Cha, M. Pasta, K. J. Koski, J. Yao, Y. Cui, *Nano Lett.* **2013**, *13*, 1341–1347.
- [124] Y. Yang, H. Fei, G. Ruan, C. Xiang, J. M. Tour, *Adv. Mater.* **2014**, *26*, 8163–8168.
- [125] M. Salanne, B. Rotenberg, K. Naoi, K. Kaneko, P. L. Taberna, C. P. Grey, B. Dunn, P. Simon, *Nat. Energy* **2016**, *1*.
- [126] J. Suntivich, K. J. May, H. A. Gasteiger, J. B. Goodenough, Y. Shao-Horn, *Science* **2011**, *334*, 1383–1385.
- [127] Y. Lee, J. Suntivich, K. J. May, E. E. Perry, Y. Shao-Horn, *J. Phys. Chem. Lett.* **2012**, *3*, 399–404.
- [128] T. Audichon, T. W. Napporn, C. Canaff, C. Morais, C. Comminges, K. B. Kokoh, *J. Phys. Chem. C* **2016**, *120*, 2562–2573.
- [129] W. Zuo, C. Xie, P. Xu, Y. Li, J. Liu, *Adv. Mater.* **2017**, *29*.
- [130] L. L. Zhang, X. S. Zhao, *Chem. Soc. Rev.* **2009**, *38*, 2520–2531.
- [131] M. Galinski, A. Lewandowski, I. Stepniak, *Electrochim. Acta* **2006**, *51*, 5567–5580.
- [132] J. Krummacher, A. Balducci, *Chem. Mater.* **2018**, *30*, 4857–4863.
- [133] M. Armand, F. Endres, D. R. Macfarlane, H. Ohno, B. Scrosati, *Nat. Mater.* **2009**, *8*, 621–629.
- [134] A. Balducci, R. Dugas, P. L. Taberna, P. Simon, D. Plée, M. Mastragostino, S. Passerini, *J. Power Sources* **2007**, *165*, 922–927.
- [135] F. Beguin, V. Presser, A. Balducci, E. Frackowiak, *Adv. Mater.* **2014**, *26*, 2219–2251.
- [136] R. D. Zhang, J. Z. Bao, Y. H. Wang, C. F. Sun, *Chem. Sci.* **2018**, *9*, 6193–6198.
- [137] A. Calhoun, G. A. Voth, *J. Phys. Chem. B* **1998**, *102*, 8563–8568.
- [138] C. J. Xu, B. H. Li, H. D. Du, F. Y. Kang, *Angew. Chem. Int. Ed.* **2012**, *51*, 933–935; *Angew. Chem.* **2012**, *124*, 957–959.
- [139] M. Y. Xia, J. H. Nie, Z. L. Zhang, X. M. Lu, Z. L. Wang, *Nano Energy* **2018**, *47*, 43–50.

Manuscript received: September 3, 2018

Accepted manuscript online: October 15, 2018

Version of record online: November 15, 2018